

Optimization of an *m*= 0 multi-loop helicon source configuration for linear plasma devices: A comparative study with Boswell and half-helix antenna designs

Yi Yu(余羿), Hao Liu(刘灏), Xue-Dong Huang(黄学栋), Chen-Yu Xiao(肖晨雨), Lin Nie(聂林), Guang-Yi Zhao(赵光义), and Min Xu(许敏)

Citation: Chin. Phys. B, 2025, 34 (**12**): 125202. DOI: 10.1088/1674-1056/ade24b
http://cpb.iphy.ac.cn; http://iopscience.iop.org/cpb

What follows is a list of articles you may be interested in

New progress on DC H_2^+ beam generation: Tens of mA output and 70% fraction from a 2.45 GHz microwave driven ion source

Bujian Cui(崔步坚), Shixiang Peng(彭士香), Jianbin Zhu(朱建斌), Yicheng Dong(董宜承), Zhiyu Guo(郭之虞), and Jiaer Chen(陈佳洱)

Chin. Phys. B, 2025, 34 (**8**): 085203. DOI: 10.1088/1674-1056/adf1ec

Power transfer efficiency in an air-breathing radio frequency ion thruster

Gao-Huang Huang(黄高煌), Hong Li(李宏), Fei Gao(高飞), and You-Nian Wang(王友年)

Chin. Phys. B, 2024, 33 (**7**): 075201. DOI: 10.1088/1674-1056/ad426c

Numerical studies for plasmas of a linear plasma device HIT-PSI with geometry modified SOLPS-ITER

Min Wang(王敏), Qiuyue Nie(聂秋月), Tao Huang(黄韬), Xiaogang Wang(王晓钢), and Yanjie Zhang(张彦杰)

Chin. Phys. B, 2024, 33 (**3**): 035204. DOI: 10.1088/1674-1056/ad16d4

Transition from a filamentary mode to a diffuse one with varying distance from needle to stream of an argon plasma jet

Hui-Min Xu(许慧敏), Jing-Ge Gao(高敬格), Peng-Ying Jia(贾鹏英), Jun-Xia Ran(冉俊霞), Jun-Yu Chen(陈俊宇), and Jin-Mao Li(李金懋)

Chin. Phys. B, 2024, 33 (**1**): 015205. DOI: 10.1088/1674-1056/ad0149

Preliminary computation of the gap eigenmode of shear Alfvén waves on the LAPD

Lei Chang(苌磊)

Chin. Phys. B, 2018, 27 (**12**): 125201. DOI: 10.1088/1674-1056/27/12/125201

Optimization of an $m = 0$ multi-loop helicon source configuration for linear plasma devices: A comparative study with Boswell and half-helix antenna designs

Yi Yu(余羿)[1,†], Hao Liu(刘灏)[2,‡], Xue-Dong Huang(黄学栋)[1], Chen-Yu Xiao(肖晨雨)[1], Lin Nie(聂林)[2], Guang-Yi Zhao(赵光义)[2], and Min Xu(许敏)[2]

[1] *Sino-French Institute of Nuclear Engineering and Technology, Sun Yat-sen University, Zhuhai* 519082, *China*
[2] *Southwestern Institute of Physics, Chengdu* 610041, *China*

(Received 28 March 2025; revised manuscript received 28 May 2025; accepted manuscript online 9 June 2025)

This article presents the physics for determining an appropriate helicon plasma source for the linear experimental advanced device (LEAD) through tripartite mutual verification encompassing theoretical analysis, code simulation, and experimental validation. Using the HELIC code, plasma excitation processes were simulated with three antenna configurations: $m = 1$ half-helix, $m = 1$ Boswell, and $m = 0$ single-loop helicon antennas, and complemented by theoretical analysis. Key parameters including plasma impedance ($R_{\rm p}$) and energy deposition profiles along radial (P_r) and axial (P_z) directions were comparatively analyzed, revealing significantly enhanced $R_{\rm p}$, P_r, and P_z values for the loop antenna configuration as compared with other configurations. Wave propagation equation solutions predicted a primary plasma generation layer at the antenna center; numerical simulations identified an additional plasma formation region at the antenna boundary, indicative of edge Landau damping effects. Interestingly, stronger axial magnetic fields do not necessarily result in higher plasma densities, especially for $m = 0$ antenna configurations. Experimental validation conducted with an $m = 0$ multi-loop plasma source confirmed these findings. Both theoretical analyses and experimental studies on large-volume plasma generation utilizing this innovative source elucidated the underlying mechanisms responsible for the remarkable low mode transition threshold of 150-watt input power and demonstrated significantly enhanced plasma confinement properties.

Keywords: multi-loop helicon source, $m = 0$ helicon source, linear plasma device

PACS: 52.50.Dg, 52.50.Qt, 52.75.–d

DOI: 10.1088/1674-1056/ade24b **CSTR:** 32038.14.CPB.ade24b

1. Introduction

Compact plasma devices serve as valuable auxiliary systems that complement large-scale fusion facilities such as tokamaks and stellarators. Linear plasma devices have gained prominence not only for plasma-material interaction studies but also for fundamental plasma physics research. Unlike tokamaks, linear devices require external plasma generation within their vacuum chambers. The critical component enabling this is the plasma source unit, with various configurations including hot cathode sources,[1] arc discharge sources,[2] and microwave-driven sources.[3] Among these, helicon plasma sources have emerged as particularly effective.

The development of helicon sources originated from Lehane's pioneering work,[4] operating through a distinct energy transfer mechanism: injected radio-frequency (RF) waves undergo mode conversion from inductively-coupled electromagnetic oscillations to helicon wave propagation, accompanied by enhanced RF power absorption. The system's performance critically depends on antenna efficiency, which determines the effectiveness of RF-to-plasma energy coupling. Various antenna configurations have been implemented in linear devices, with notable designs including the Nagoya type III,[5] Boswell,[6] and half-helix[7] antennas — all characterized by azimuthal mode number $m = 1$. While the fundamental $m = 0$ configuration (simple loop antenna) appears conceptually straightforward,[8] its application remained underreported until recent successful implementations in plasma processing testbed (PPT)[9] and plasma assembly for non-linear turbulence analysis (PANTA)[10] experiments.

Conventional helicon sources typically employ a dielectric (glass/quartz) discharge tube concentrically surrounded by the antenna structure, forming an integral part of the vacuum system. Shinohara's innovative flat-spiral metallic antenna design[11,12] eliminated the dielectric tube, offering practical advantages for out-vacuum maintenance and positional adjustments without breaking the vacuum vessel. Despite the widespread adoption of helicon sources, a systematic comparative analysis of $m = 0$ versus higher-order mode antennas is still lacking, especially in the context of tripartite validation through theoretical modeling, numerical simulations, and experimental verification.[13]

This study presents an $m = 0$ helicon plasma source em-

†Corresponding author. E-mail: yuyi56@mail.sysu.edu.cn
‡Corresponding author. E-mail: liuhao@swip.ac.cn

© 2025 Chinese Physical Society and IOP Publishing Ltd. All rights, including for text and data mining, AI training, and similar technologies, are reserved.

ploying a planar multi-loop antenna design, developed through comprehensive electromagnetic simulations and theoretical analysis of wave energy deposition characteristics across different antenna configurations. The optimized antenna system exhibits enhanced coupling efficiency, producing azimuthally symmetric plasma modes.

2. Experimental setup

The linear experimental advanced device (LEAD) represents a medium-scale linear plasma facility with unique structural characteristics (Fig. 1(e)). The system features a distinctive two-segment cylindrical configuration comprising dual vacuum chambers with respective inner diameters of 400 mm and 900 mm, interconnected through a gradual conical stainless steel transition section. The primary vacuum chamber (400 mm diameter) incorporates specially designed plasma limiters that enable dynamic control of plasma column confinement. Through adjustable limiter configurations, the operational plasma diameter can be precisely regulated within a 100–400 mm range to meet specific experimental requirements.

Prior to the construction of the LEAD device, two prevalent $m = 1$ helicon antenna configurations — the Boswell-type (Fig. 1(a)) and half-helix type (Fig. 1(b)) — underwent comprehensive evaluation. The HELIC code is a classical program for designing helicon antennas, focusing on analyzing electromagnetic wave propagation in cold plasma. Although more advanced programs such as COMSOL multiphysics can simulate detailed helicon discharge dynamics, the HELIC program provides a quick, simple, and straightforward method to evaluate antenna behavior under user-specified plasma parameters. Numerical simulations employing the HELIC code[14] were conducted for both antenna designs, incorporating actual LEAD operational parameters including vacuum vessel dimensions, magnetic field strength B_0, and target plasma density n_e. For comparative analysis, simulations also included the fundamental $m = 0$ single-loop configuration (Fig. 1(c)).

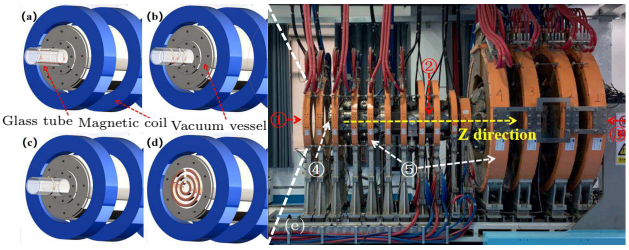


Fig. 1. Schematic of the plasma source configuration at the left terminus of LEAD, featuring four helicon antenna candidates: (a) $m = 1$ mode Boswell antenna; (b) $m = 1$ mode half-helix antenna; (c) $m = 0$ mode single-loop antenna; (d) $m = 0$ mode flat multi-loop antenna (quartz tube excluded). (e) Operational schematic: ① The multi-loop helicon source maintains axial mobility (red arrow) for optimal coupling with the vacuum vessel's quartz window ④; ② diagnostic access port for Langmuir probe insertion to measure plasma density; ③ fast-framing camera aligned with the axial viewing direction (red arrow); ⑤ orange-colored magnetic confinement coils. The yellow dashed arrow indicates the axial Z coordinate direction.

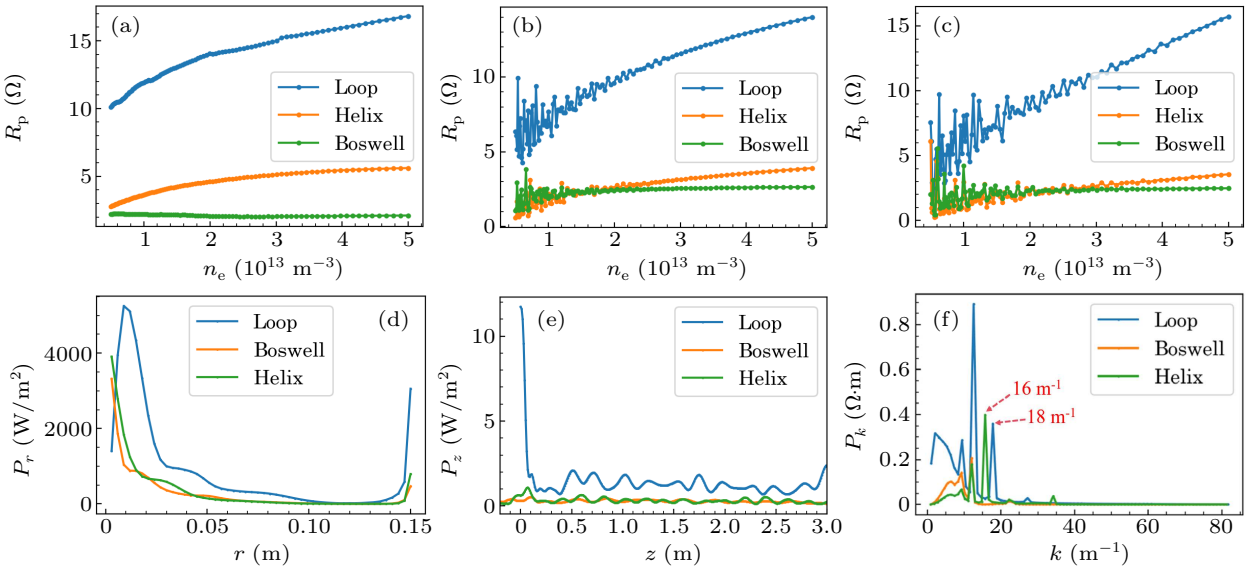


Fig. 2. (a)–(c) Comparative analysis of plasma impedance R_p across three antenna configurations under axial magnetic fields B_0 of 200 G, 1000 G, and 1500 G, respectively. (d)–(f) Energy deposition: (d) radial profiles P_r, (e) axial profiles P_z, and (f) spectral dependence P_k as a function of axial wavenumber k_z.

Figures 2(a)–2(c) present comparative analyses of plasma impedance R_p for the three antenna configurations under axial magnetic fields B_0 of 200 G, 1000 G, and 1500 G, respectively. Notably, the $m = 0$ loop antenna demonstrates considerably higher R_p values across all magnetic field intensities compared to its $m = 1$ counterparts. However, this configuration exhibits an inverse relationship with magnetic field strength, showing marked R_p reduction as B_0 increases. The Boswell antenna displays moderate enhancement proportional to the magnetic field, whereas the half-helix antenna maintains

stable impedance across the tested B_0 range. This comparative study reveals that $m = 1$ antennas generally exhibit much lower R_p sensitivity to magnetic field variations compared to the $m = 0$ loop design. Despite its B_0-dependent impedance characteristics, the loop antenna maintains a clear advantage in plasma excitation efficiency for LEAD applications.

In addition, with increasing axial magnetic field, R_p under low-density conditions exhibits significant fluctuations. This suggests that the discharge could become unstable in high magnetic fields due to potential plasma instabilities. Experiments also show that the plasma scintillates for $B > 1000$ G.

2.1. Theoretical interpretation

For helicon waves propagating in a cylindrical plasma column, the magnetic field components can be expressed as[15]

$$\begin{cases} B_r = A\left[(k+k_z)J_{m-1}(k_r r) + (k-k_z)J_{m+1}(k_r r)\right], \\ B_\theta = \mathrm{i}A\left[(k+k_z)J_{m-1}(k_r r) - (k-k_z)J_{m+1}(k_r r)\right], \\ B_z = -2\mathrm{i}AJ_m(k_r r), \end{cases} \tag{1}$$

where B_r is the radial magnetic component, B_θ is the azimuthal magnetic component, B_z is the axial magnetic component, A is the amplitude, k is the total wavenumber, k_r is the radial component of k, k_z is the axial component of k, and J_m is the m-th order Bessel function.

For the configuration shown in Figs. 1(a)–1(c), where the helicon source consists of a quartz tube surrounded by an antenna, the insulating boundary condition requires the radial magnetic field to vanish at the boundary

$$B_r(r = a) = mkJ_m(k_r a) + k_z J_m'(k_r a) = 0.$$

For the $m = 0$ mode (using a copper loop antenna with radius $a = 150$ mm), this simplifies to

$$J_0'(k_r a) = 0,$$

yielding the lowest radial mode solution

$$k_r = \frac{3.83}{a} = 25.53\ \mathrm{m}^{-1}. \tag{2}$$

The energy deposition can be expressed as

$$\langle j_z E_z \rangle = \frac{2A^2\gamma_{\mathrm{eff}}}{\varepsilon_0\omega_p^2}\left(\frac{k}{\mu_0}k_r J_m(k_r r)\right)^2, \tag{3}$$

where j_z is the axial current density, E_z is the axial electric field, ω_p is the plasma angular frequency, and γ_{eff} is the total effective collision frequency.

Equation (3) predicts concentrated energy deposition at the plasma core ($r \to 0$) for the $m = 0$ mode, consistent with the prominent central peak observed in Fig. 2(d) for the $m = 0$ loop antenna. However, the secondary deposition region near the tube edge ($r = a$) deviates from this prediction, which can be attributed to edge heating through Landau damping,[16] to be experimentally verified in subsequent sections.

The plasma dispersion relation is given by[17]

$$kk_z = \sqrt{k_r^2 + k_z^2}\cdot k_z = \frac{e\mu_0 n_e \omega}{B_0}. \tag{4}$$

Through simultaneous solution of Eqs. (1) and (3), two key relationships emerge: ① reduced antenna diameter a enhances plasma density under constant axial wavenumber k_z and magnetic field B_0 conditions; ② increased k_z elevates plasma density within fixed tube size and B_0.

Figure 2(f) presents the simulated k_z-dependence of energy deposition P_k. The $m = 0$ loop antenna exhibits a distinct P_k maximum at $k_z \approx 18\ \mathrm{m}^{-1}$, significantly exceeding the $m = 1$ antenna values. This aligns with conclusion ② and explains the superior energy deposition efficiency of $m = 0$ configurations shown in Figs. 2(a)–2(e). Comparative analysis of $m = 1$ antennas reveals the half-helix design achieves higher P_k (peaking at $k_z \approx 16\ \mathrm{m}^{-1}$) than the Boswell-type, consistent with its enhanced deposition performance in Figs. 2(a)–2(e).

2.2. Experimental results

2.2.1. Source developing

Following comprehensive analysis of antenna performance through numerical simulations and theoretical considerations regarding $m = 0$ loop, $m = 1$ helix, and $m = 1$ Boswell configurations, the $m = 0$ loop antenna was selected for the LEAD experiment. This decision was based on its superior impedance (R_p) characteristics, enhanced energy deposition capabilities ($P_r/P_{r,\mathrm{total}}$ and P_k), and structural simplicity. Drawing inspiration from Shinohara's spiral antenna design,[11] we developed an $m = 0$ helicon source featuring a concentric circular loop antenna (Figs. 1(d) and 3(a)).

The final implementation comprises four concentric copper loops with progressively increasing diameters of 80 mm, 160 mm, 240 mm, and 320 mm. Unlike conventional designs that surround quartz tubes, this antenna is positioned externally in direct contact with the vacuum-sealed 340-mm quartz window (component ④ in Fig. 1(e)) at LEAD's terminal end. This innovative configuration achieves complete vacuum isolation without any direct vacuum connection to the vessel while incorporating integrated water cooling channels for thermal management during operation. The modular design permits flexible electrical connections between loops via adjustable copper busbars, though the outermost 320-mm loop remained disconnected in the present experiments to prevent arcing with the 340-mm quartz window periphery.

2.2.2. Results and interpretation

Figure 3(b) demonstrates typical plasma discharge patterns under moderate power input (hundreds of Watts) using the three inner loops. The observed luminous structures —

three distinct concentric rings and a central bright spot — exhibit precise spatial correlation with antenna geometry. These features provide direct experimental validation of the simulated energy deposition profile shown in Fig. 2(d), confirming two key mechanisms: ① peripheral heating through Landau damping (manifested as annular patterns matching loop positions); ② central power deposition predicted by Eq. (3) solutions. Notably, all luminous features localize near the quartz window's vacuum interface ($z \approx 0$ region), experimentally corroborating the theoretical deposition profile in Fig. 2(e). The characteristic blue-core emission spectrum further confirms wave-driven discharge operation.

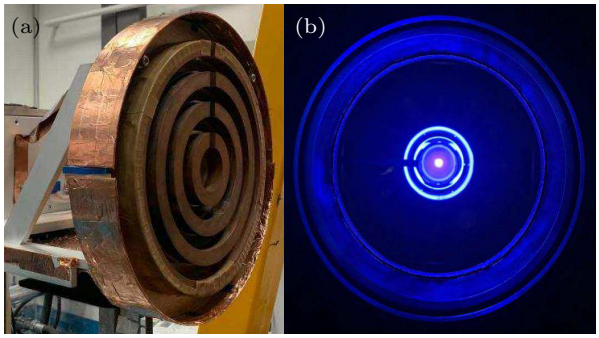


Fig. 3. (a) Multi-loop antenna configuration implemented on LEAD. (b) Captured discharge phenomenon exhibiting three distinct bright circular bands with a central bright spot.

It should be emphasized that the previous analysis employing Eq. (1) assumes an insulating boundary condition, specifically derived for the single-loop configuration where the loop encircles an insulating quartz tube. This configuration imposes the radial magnetic field condition

$$\begin{aligned} B_r(r=a) &= A\left[(k+k_z)J_{m-1}(k_r r)+(k-k_z)J_{m+1}(k_r r)\right] \\ &= 0. \end{aligned} \tag{5}$$

For the multi-loop antenna system, however, the loops are externally mounted on a vacuum vessel with a diameter of 400 mm, significantly larger than the loop dimensions. Crucially, the three distinct plasma bands observed in Fig. 3(b) lack an insulating quartz boundary. Instead, each loop (or equivalently, each plasma band) must satisfy a conducting boundary condition, as plasmas inherently behave as conductors. This requires the azimuthal electric field to vanish at the boundary: $E_\theta(r=a)=0$. By invoking the field transformation relation $E_\theta = (-\omega A/k)B_r$, this condition translates to

$$\begin{aligned} E_\theta(r=a) &= (-\omega A/k)\Big[(k+k_z)J_{m-1}(k_r r) \\ &\quad +(k-k_z)J_{m+1}(k_r r)\Big] = 0. \end{aligned} \tag{6}$$

Notably, this equation is mathematically identical to Eq. (5). Consequently, the physical interpretation derived from the single-loop insulating boundary condition remains valid for the multi-loop antenna system, despite the transition to a conducting plasma boundary.

2.2.3. Comparison experiments

A multi-ring antenna with flexible connections between four concentric rings was built to compare different antenna configurations in further studies. In this article, most experimental results are obtained with a multi-loop configuration in which the three inner rings are connected in series. We compare the density profiles between single-loop and multi-loop configurations. A conventional $m=0$ loop helicon source with 170 mm diameter has been installed on the left port of the LEAD vacuum vessel as a reference configuration for comparative plasma generation studies.

Figure 4 presents radial plasma density profiles obtained from both antenna configurations under comparable operational conditions: argon working gas at 0.7 Pa pressure, 2 kW RF power input, and 1000 Gauss axial magnetic field. The density measurements were acquired using a mid-plane Langmuir triple probe inserted through the side diagnostic port (location ② in Fig. 1(e)).

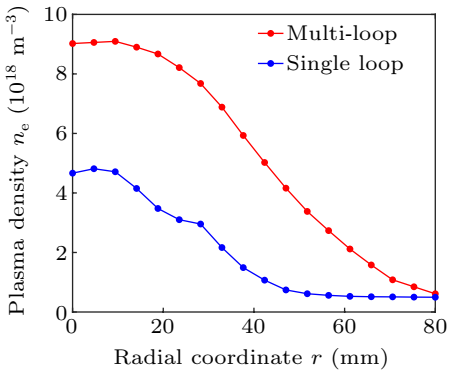


Fig. 4. Comparative density profiles of LEAD plasma generated by conventional single-loop (blue) and multi-loop (red) helicon antenna configurations.

The comparative analysis reveals significantly enhanced plasma density generation by the multi-loop antenna despite equivalent power input, indicating superior plasma excitation efficiency and improved antenna-plasma energy coupling. The multi-loop configuration comprises three concentric loops with radii $a_1 = 80$ mm, $a_2 = 160$ mm, and $a_3 = 240$ mm. Applying Eq. (2), the corresponding radial wavenumbers are calculated as $k_{r1} \approx 48.78$ m^{-1}, $k_{r2} \approx 23.94$ m^{-1}, and $k_{r3} = 15.96$ m^{-1}. Notably, the dominant k_{r1} and k_{r2} components substantially exceed the conventional single-loop value of $k_r = 3.83/0.17$ m^{-1} $= 22.53$ m^{-1} (derived from Eq. (4)), while maintaining equivalent axial wavenumber k_z. This enhanced radial wavenumber spectrum provides the physical mechanism for the observed density improvement.

Notably, in plasma excitation governed by Eq. (4), the axial wavenumber k_z demonstrates greater dominance over the radial component k_r. Unlike $m=1$ antenna configurations where k_z is structurally constrained along the axial direction, the $m=0$ loop and multi-loop antennas permit unrestricted k_z values. This inherent flexibility in wavenumber selection

potentially enables $m = 0$ helicon sources to generate higher plasma densities, as evidenced by the comparative analysis in Figs. 2(a)–2(e).

However, the unconstrained nature of k_z in $m = 0$ configurations may introduce operational complexities. The observed impedance reduction R_p with increasing magnetic field in Figs. 2(a)–2(c) suggests significant k_z variations. This phenomenon provides a possible explanation for the non-monotonic plasma density dependence on B_0 observed in LEAD magnetic field scanning experiments (Fig. 5), which deviates from the conventional predictions of Eq. (4). The results in Fig. 5 are restricted to 200–1250 G due to the achievable stable discharge limit (1250 G). Exceeding this threshold induces plasma instability. In contrast, $m = 1$ antenna systems exhibit more stable performance characteristics due to their fixed k_z values, as demonstrated by the relatively weaker R_p dependence on B_0 shown in Figs. 2(a)–2(c).

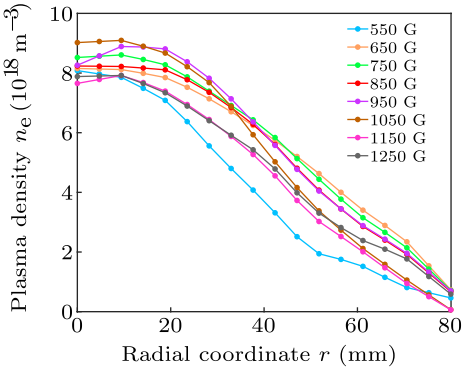


Fig. 5. Evolution of density distribution characteristics in LEAD plasma under varying magnetic flux density B_0. The plasma density exhibits a positive correlation with B_0 of lower than 850 G.

3. Discussion and conclusion

The $m = 0$ multi-loop helicon source serves as the primary plasma generation system in the LEAD experiment. By leveraging the distinct plasma excitation characteristics of concentric loops with varying dimensions, this innovative source achieves steady-state plasma densities up to 4×10^{19} m^{-3} at an axial position $z = 1.5$ m from the source plane, operating at 6 kW RF power with argon background pressure maintained at 1.95 Pa.

Numerical simulations and theoretical analyses provide dual insights: they elucidate both the plasma excitation efficiency variations among different helicon antenna configurations and the characteristic density profiles generated by the $m = 0$ multi-loop design. These findings establish a framework for systematic performance enhancement for the $m = 0$ multi-loop helicon source.

The antenna's operational superiority stems from its unique $m = 0$ excitation geometry (as predicted by Eq. (3) and illustrated in Fig. 2(d)), which enables two critical features: ① efficient mode transition of large-volume plasmas from inductive coupling to helical wave propagation at remarkably low power thresholds ($\sim$ 150 W); ② plasma generation efficiency reaching 30×10^{13} W^{-1}, approaching the theoretical upper limit predicted by scaling laws.[18]

This multi-loop architecture creates distributed edge energy deposition layers through sequential loop interconnection. The self-regulating power distribution among loops indicates optimal impedance matching and plasma-wave coupling for each individual loop. This synergistic configuration enables multi-layered plasma generation, producing steady-state large-volume plasmas with enhanced radial uniformity which improves confinement and suppresses turbulent transport through minimization of radial density gradients.[19]

Acknowledgments

Project supported by the National Key Research and Development Program of China (Grant No. 2022YFE03100002) and the National Natural Science Foundation of China (Grant Nos. 12435015 and 12075241).

References

[1] Antonov N N, Usmanov R A, Gavrikov A V and Smirnov V P 2019 *J. Phys.: Conf. Ser.* **1147** 012133
[2] van Eck H J N, Abrams T, van den Berg M A, *et al.* 2014 *Fusion Eng. Des.* **89** 2150
[3] Cojocaru G 2000 *Rev. Sci. Instrum.* **71** 966
[4] Lehane J A and Thonemann P C 1965 *Proc. Phys. Soc.* **85** 301
[5] Okamura S, Adati K, Aoki T, Baker D R, Fujita H, Garner H R, Hattori K, Hidekuma S, Kawamoto T, Kumazawa R, Okubo Y and Sato T 1986 *Nucl. Fusion* **26** 1491
[6] Boswell R W 1970 *Phys. Lett.* **33A** 457
[7] Miljak D G and Chen F F 1998 *Plasma Sources Sci. Technol.* **7** 61
[8] Seto T, Ezumi N, Miyauchi R, Shigematsu N, Okamoto T, Takahashi S, *et al.* 2023 *Plasma Fusion Res.* **18** 2401054
[9] Xu T C, Yang X Y, Guo Z B, Xiao C J, Wang X G and He R C 2020 *Nucl. Fusion* **60** 016029
[10] Oldenburger S, Inagaki S, Kobayashi T, Arakawa H, Ohyama N, Kawashima K, Tobimatsu Y, Fujisawa A, Itoh K and Itoh S I 2012 *Plasma Phys. Control. Fusion* **54** 055002
[11] Shinohara S, Takechi S and Kawai Y 1996 *Jpn. J. Appl. Phys.* **35** 4503
[12] Shinohara S 2018 *Adv. Phys. X* **3** 14204243
[13] Takahashi K, Chiba A, Komuro A, *et al.* 2015 *Phys. Rev. Lett.* **114** 195001
[14] Arnush D 2000 *Phys. Plasmas* **7** 3042
[15] Chen F F 1991 *Plasma Phys. Control. Fusion* **33** 339
[16] Kline J L, Scime E E, Boivin R F, Keesee A M and Sun X 2002 *Phys. Rev. Lett.* **88** 195002
[17] Chabert P and Braithwaite N 2011 *Physics of radio-frequency plasmas* (Cambridge: Cambridge University Press) p. 272
[18] Shinohara S, Hada T, Motomura T, Tanaka K, Tanikawa T, Toki K, Tanaka Y and Shamrai K P 2009 *Phys. Plasmas* **16** 057104
[19] Liu H, Yu Y, Xiao C Y, Yuan Z H, Wang H J, Nie L, Ke R, Long T, Gong S B and Xu M 2023 *Plasma Phys. Control. Fusion* **65** 055017